

## Two- and three-dimensional magnetic reconnection observed in the Eulerian-Lagrangian analysis of magnetohydrodynamics equations

K. Ohkitani

*Department of Applied Mathematics, School of Mathematics and Statistics, The University of Sheffield,  
Hicks Building, Hounsfield Road, Sheffield S3 7RH, United Kingdom*

P. Constantin

*Department of Mathematics, The University of Chicago, Chicago, Illinois 60637, USA*

(Received 11 June 2008; revised manuscript received 7 September 2008; published 29 December 2008)

We study reconnection phenomena in magnetohydrodynamics on the basis of a magnetohydrodynamic version of the Eulerian-Lagrangian analysis. We find that the methods are useful in capturing time scales associated with magnetic reconnection both in two and three dimensions. Visualizations show that the determinants of the Jacobian determinants of the diffusive labels are small where active reconnection takes place. The resetting of the diffusive labels extracts a short time scale during reconnection.

DOI: [10.1103/PhysRevE.78.066315](https://doi.org/10.1103/PhysRevE.78.066315)

PACS number(s): 47.65.-d, 52.65.Kj

### I. INTRODUCTION

Magnetic reconnection is a phenomenon that has been extensively investigated in magnetohydrodynamics contexts, because of its importance in plasma and solar physics [1–3]. There are a number of mathematical models that display some essential features of magnetic reconnection phenomena, especially in two-dimensional and stationary cases. On the other hand, the understanding of nonstationary three-dimensional reconnection seems to be far from being satisfactory, in spite of a lot of efforts that have been made theoretically and numerically.

In this paper, a method of detecting the magnetic reconnection is proposed and applied to some numerical simulations. This method is based on the Eulerian-Lagrangian formalism for the Navier-Stokes equations which has been developed in Refs. [4,5]. The method has been applied to numerical calculations of the Navier-Stokes equations in Ref. [6]. There it was found that the resetting phenomena associated with noninvertibility of diffusive Lagrangian maps captures vortex reconnection successfully. This formalism was also applied to the analysis of turbulence [7].

It should be noted that this formalism for the Navier-Stokes equations has been extended further by using the Moore-Penrose algorithm in solving the underdetermined system of equations for the potentials [8] and that it has been applied to number of cases. Recently, an interesting work has been done [9] on the basis of the generalized Euler-Lagrangian formulation including the magnetohydrodynamic cases. There, the diffusive labels are introduced at the level of the magnetic induction equations, by using viscous Weber transforms for the magnetic potentials. As the initial data, the three-dimensional *ABC* flow, the two- and three-dimensional Orszag-Tang vortices were treated. The main result of that work is that the frequent resettings are correlated with growth of magnetic enstrophy.

Here we attempt to characterize magnetic reconnection in the magnetohydrodynamics (MHD) systems using the original Eulerian-Lagrangian formalism, that is, without the Moore-Penrose procedure. We first formulate the generalization of

Eulerian-Lagrangian formalism for the MHD case. Then we apply it to two- and three-dimensional MHD equations numerically to study magnetic reconnection.

In our theoretical formulation, we consider viscous Weber transforms both for magnetic potentials and for velocity fields. This allows the interpretation that the diffusive labels describe reconnection phenomena both in magnetic and velocity (vorticity) fields. In this formulation, however, we are restricted to the case of unit magnetic Prandtl number. The formulation used here is more special than what was used in Ref. [9] in the sense that it does not use Moore-Penrose algorithm, but more general in the sense that both magnetic and kinetic potentials have dissipative labels. In addition to the technical issue of making both Weber potentials dissipative, there is a clear observation of predominant magnetic reconnection which converts magnetic energy into kinetic energy efficiently in a short time scale, one of the most important phenomena in plasma physics. We will show, in particular, how the diffusive labels can keep track of active magnetic reconnection in a number of typical numerical experiments, both in extracting its time scale and in identifying the locations in physical space.

The rest of this paper is organized as follows. We describe the mathematical formulation in Sec. II. In Sec. III, numerical results are presented in three and two dimensions. Section IV will be devoted to a summary and discussion.

### II. DISSIPATIVE MHD IN THREE DIMENSIONS

The Eulerian-Lagrangian formulation for the Navier-Stokes equations was developed in Ref. [4,5]. We generalize it to the case of MHD under the assumption of unit magnetic Prandtl number. To do so we recall two Weber transforms, one for velocity and the other for the magnetic potential, in ideal magnetohydrodynamics (Appendix) and make both of them dissipative.

With standard notations, a set of dissipative MHD equations reads for that case as follows:

$$\frac{D\mathbf{u}}{Dt} = -\nabla p + (\nabla \times \mathbf{B}) \times \mathbf{B} + \nu \Delta \mathbf{u}, \quad (1)$$

$$\frac{\partial \mathbf{B}}{\partial t} = \nabla \times (\mathbf{u} \times \mathbf{B}) + \nu \Delta \mathbf{B}, \quad (2)$$

and

$$\nabla \cdot \mathbf{u} = \nabla \cdot \mathbf{B} = 0. \quad (3)$$

Let the diffusive labels  $\mathbf{A}$  obey

$$\frac{D\mathbf{A}}{Dt} = \nu \Delta \mathbf{A}, \quad (4)$$

where  $\mathbf{A} = \mathbf{x}$  at  $t=0$ .

We first treat  $\tilde{\mathbf{u}}$  (see the Appendix for its definition). Set

$$\tilde{\mathbf{u}} = \mathbf{v}(\nabla \mathbf{A})^T - \nabla \phi \quad (5)$$

or, in components,

$$\tilde{u}_i = \frac{\partial A_j}{\partial x_i} v_j - \frac{\partial \phi}{\partial x_i}. \quad (6)$$

(Equivalently, we may write  $\mathbf{u} = \mathbf{P}[\mathbf{v}(\nabla \mathbf{A})^T + \mathbf{m} \times \mathbf{B}]$ , where  $\mathbf{m}$  is defined in Eq. (10) below.) If

$$\frac{D\mathbf{v}}{Dt} = \nu \Delta \mathbf{v} + 2\nu \mathbf{C} : \nabla \mathbf{v}, \quad (7)$$

where  $\mathbf{C}$  is defined as usual by  $C_{m,k;i} = Q_{ji} \partial_j \partial_k A_m$  with  $\mathbf{Q} = (\nabla \mathbf{A})^{-1}$ . Then it can be shown that

$$\frac{D\tilde{\mathbf{u}}}{Dt} = -\nabla p - (\mathbf{B} \times \mathbf{m}) \cdot (\nabla \mathbf{u})^T + \nu \Delta \tilde{\mathbf{u}} \quad (8)$$

and

$$\frac{D\phi}{Dt} = p - \frac{|\mathbf{u}|^2}{2} + \nu \Delta \phi. \quad (9)$$

The equation for  $\mathbf{m}$  takes the following form

$$\frac{D\mathbf{m}}{Dt} = \mathbf{m} \cdot \nabla \mathbf{u} + \mathbf{J} + \nu \Delta \mathbf{m} + \nu \frac{(\nabla |\mathbf{B}|^2 \cdot \nabla) \mathbf{m}}{|\mathbf{B}|^2}. \quad (10)$$

(See the Appendix for the definition of  $\mathbf{J}$ .)

Second, we consider the magnetic potential  $\mathcal{A}$ , ( $\mathbf{B} = \nabla \times \mathcal{A}$ ). Note that  $\mathcal{A}$  is to be distinguished from  $\mathbf{A}$ . For this easier part, we set

$$\mathcal{A} = \mathbf{P}[\mathbf{W}(\nabla \mathbf{A})^T] \quad (11)$$

or

$$\mathcal{A}_i = \frac{\partial A_j}{\partial x_i} W_j - \frac{\partial \psi}{\partial x_i}. \quad (12)$$

If we assume that the equation for  $\mathbf{W}$  is given by

$$\frac{D\mathbf{W}}{Dt} = \nu \Delta \mathbf{W} + 2\nu \mathbf{C} : \nabla \mathbf{W}, \quad (13)$$

with the same  $\mathbf{C}$ , then we have

$$\frac{D\mathcal{A}}{Dt} = \nu \Delta \mathcal{A} - \mathcal{A}(\nabla \mathbf{u})^T - \nabla \chi \quad (14)$$

and

$$\frac{D\psi}{Dt} = \chi + \nu \Delta \psi. \quad (15)$$

Thus the set of equations (4), (7), and (13) constitutes an alternative representation  $(\mathbf{A}, \mathbf{v}, \mathbf{W})$  for MHD, which is equivalent to  $(\mathbf{u}, \mathbf{B})$ .

### III. NUMERICAL RESULTS

#### A. Numerical method

Practically, we solve the following set of equations for the impulse  $\gamma$  and the magnetic field  $\mathbf{B}$ :

$$\frac{\partial \gamma}{\partial t} = \mathbf{u} \times \boldsymbol{\omega} + (\mathbf{B} \cdot \nabla) \mathbf{B} + \nu \Delta \gamma, \quad (16)$$

$$\frac{\partial \mathbf{B}}{\partial t} = \nabla \times (\mathbf{u} \times \mathbf{B}) + \nu \Delta \mathbf{B}, \quad (17)$$

and

$$\frac{D\mathbf{l}}{Dt} = -\mathbf{u} + \nu \Delta \mathbf{l}. \quad (18)$$

Here  $\mathbf{l}$  denotes displacement

$$\mathbf{l} \equiv \mathbf{A} - \mathbf{x} \quad (19)$$

and the incompressible velocity field is retrieved from impulse  $\gamma$  by solenoidal projection

$$\mathbf{u} = \mathbf{P}[\gamma]. \quad (20)$$

Note that we have  $\gamma = \mathbf{v}(\nabla \mathbf{A})^T + \mathbf{m} \times \mathbf{B}$  (modulo a scalar gradient).

Under periodic boundary conditions, we solve the above equations by pseudospectral methods. We use  $256^3$  grid points, with aliasing errors removed by the 2/3 rule. Time marching was done by Runge-Kutta scheme.

If the correspondence between  $\mathbf{A}$  and  $\mathbf{x}$  becomes noninvertible, that is, when  $\det(\nabla \mathbf{A})$  becomes very small, we reset  $\mathbf{A}$  as  $\mathbf{A} = \mathbf{x}$ . In practice we adopt the following:

$$\text{Det}(\nabla \mathbf{A}) \leq \epsilon \Rightarrow \mathbf{l} = \mathbf{0}$$

as a resetting criterion typically with  $\epsilon = 0.01$ . In this way we describe the MHD fields in terms of near-identity transformations.

#### B. Three-dimensional MHD

It is important choose initial condition appropriately for magnetic reconnection to take place. Here we consider magnetic fields made up of a number of compactly supported magnetic flux tubes.

By the extensive numerical studies on magnetic reconnection done so far, it is now understood that at least two factors should be taken into account for efficient reconnection, that is, (1) twists along flux tubes and (2) counterhelicity (as opposed to co-helicity) configuration in the interaction zone. It is in order to recall that a twisted flux tube has a magnetic helicity  $H$  defined by

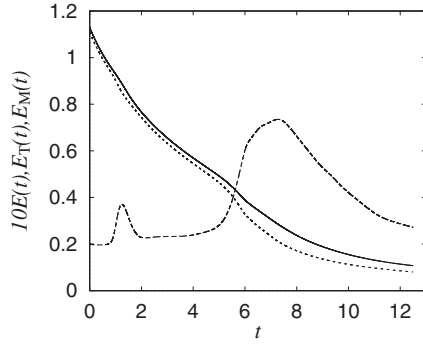


FIG. 1. Time evolution of the total energy  $E_T(t)$  (solid line), (ten times) the kinetic energy  $10E(t)$  (dashed), and the magnetic energy  $E_M(t)$  (dotted) for IC-1 with  $\nu=2.0 \times 10^{-3}$ .

$$H = \int_V \mathcal{A} \cdot \mathbf{B} dx,$$

where  $\mathbf{B} = \nabla \times \mathcal{A}$  and  $V$  is the support of  $\mathbf{B}$ . For a right-(left-) handed flux tube, the helicity  $H$  is positive (negative). A pair of tubes with helicities of the same (opposite) sign is called cohelical (counterhelical).

Each elementary flux tube of the initial fields is assumed to have Gold-Hoyle tube [10], which is given in cylindrical coordinates by

$$B_z(r) = \frac{B_0}{1 + q^2 r^2}, \tag{21}$$

$$B_\phi(r) = qrB_z(r), \tag{22}$$

where  $B_0 = 4\sqrt{8\pi} \approx 20$ , the value for  $B_0$  was taken over from a compressible case where a thermodynamic balance was used [11,12]. The parameter  $q$  denotes twist (pitch), which means azimuthal field lines wind  $q$  times in a right handed sense per a length of  $2\pi$  along the tube axis. The model of Gold and Hoyle [10] proposed for flares shows how two antiparallel flux tubes with opposite twists come into contact and reconnect in such a way that left-handed lines connect to right-handed ones and untwist themselves.

As mentioned above, a right-handed flux tube has the positive helicity and left-handed one has the negative helicity. More specifically, if the magnetic field is made up of

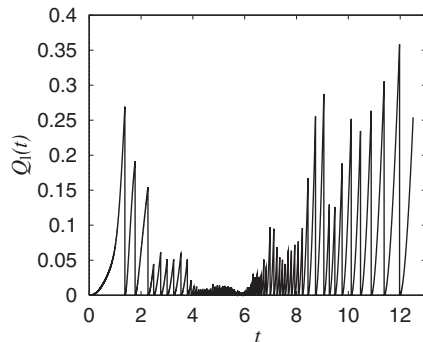


FIG. 2. Time evolution of spatial average of squared displacement for IC-1 with  $\nu=2.0 \times 10^{-3}$ .

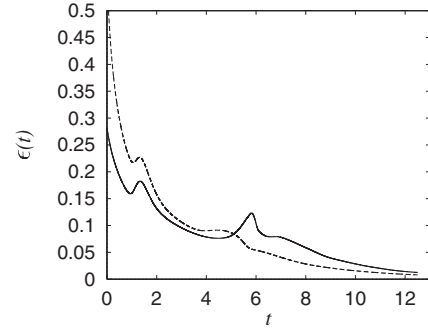


FIG. 3. Time evolution of dissipation of total energy for IC-1, for  $\nu=2.0 \times 10^{-3}$  (solid) and  $4.0 \times 10^{-3}$  (dashed).

predominant  $B_z$  and azimuthal  $B_\phi$ , it has positive (negative) helicity, depending on  $A_\phi B_\phi > 0 (< 0)$ , where  $A_\phi$  is the vector potential which is induced by  $B_z$ . The flux tube pairs are cohelical (counterhelical) when their helicities have the same (opposite) sign.

We will use three different kinds of initial conditions, taken from the comprehensive work [13]. We will address reconnection on the basis of the Eulerian-Lagrangian formalism and readers should consult Ref. [13] for the detailed descriptions of reconnection mechanisms. See also Ref. [14,15] for related issues.

For the kinematic viscosity  $\nu$  and magnetic diffusivity  $\eta$ , we use  $\nu(=\eta)=2.0 \times 10^{-3}$  and  $4.0 \times 10^{-3}$ . We treat only the case of unit magnetic Prandtl number. For the time step, we use  $\Delta t=2.5 \times 10^{-4}$  for  $t \leq 2.5$ ,  $5.0 \times 10^{-4}$  for  $t \geq 2.5$ . In the early stage, we need to make the time step smaller to stabilize the abrupt evolution associated with rapid magnetic reconnection.

As for an initial condition of velocity we take

$$\mathbf{u}(\mathbf{x}) = u_0 \{-\sin(x - \pi)[\cos(y - \pi) + \cos(z - \pi)], \\ \cos(x - \pi)\sin(y - \pi), \cos(x - \pi)\sin(z - \pi)\},$$

where  $u_A=0.2 (\approx u_A/28)$ . This is to push the flux tubes toward the origin, to trigger close interaction between them.

*IC-1: Orthogonally offset flux tubes.* This may be regarded as a magnetic counterpart of the orthogonally offset vortex tube reconnection experiment used in Ref. [16]. It is categorized as the case “slingshot” and labeled “RL2” in Ref.

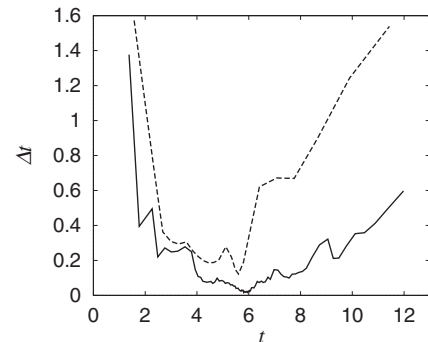


FIG. 4. Time evolution of resetting time scales for IC-1, plotted with the same line convention as in Fig. 3.

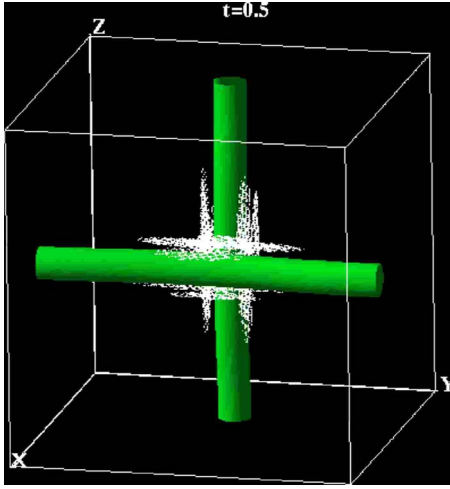


FIG. 5. (Color online) Isosurface plots of  $|\mathbf{B}|^2=39.8$  for IC-1. White dots:  $\det(\nabla\mathbf{A})=0.995$  (14 650 points).

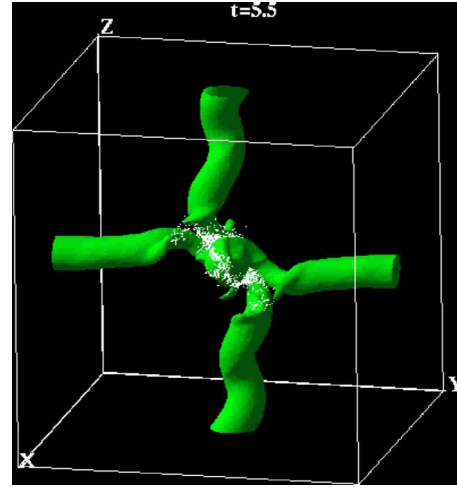


FIG. 7. (Color online) Isosurface plots of  $|\mathbf{B}|^2=16.3$  for IC-1. White dots:  $\det(\nabla\mathbf{A})=0.95$  (6683 points).

[13] (see its Fig. 10). As stressed above, for efficient reconnection of magnetic flux tubes, it is necessary for them to have twists along the field lines.

We define three kinds of energies by

$$E_T(t) = \frac{1}{2} \langle |\mathbf{u}|^2 + |\mathbf{B}|^2 \rangle,$$

$$E_M(t) = \frac{1}{2} \langle |\mathbf{B}|^2 \rangle,$$

and

$$E_K(t) = \frac{1}{2} \langle |\mathbf{u}|^2 \rangle,$$

where the brackets denote a spatial average in  $[0, 2\pi]^3$ .

In Fig. 1, we show how the total energy  $E_T(t)$  and magnetic energy  $E_M(t)$  decay in time together with an increase in kinetic energy  $E_K(t)$ . The abrupt increase in  $E_K(t)$  during 4

$\leq t \leq 8$  is due to the conversion of magnetic energy into kinetic energy via the Lorenz force term. In Fig. 2, time evolution a squared norm  $Q_1(t)$  of displacement  $\ell$  is shown, where

$$Q_1(t) = \frac{1}{2} \langle |\nabla \times \ell|^2 \rangle.$$

The curve hits zero many times as a result of resettings  $\ell = 0$ . We observe that a very frequent process of resettings is correlated with the growth of the kinetic energy (see Fig. 1).

In principle, the time evolution of diffusive labels depends on the threshold  $\epsilon$  for resetting. We have checked that the time interval with frequent resetting (e.g., as seen in Fig. 2) is insensitive to the choice of  $\epsilon$ , say in the range of 0.1-0.001 (not shown). Thus, checking resetting procedures gives a robust measure of reconnection qualitatively (see also Ref. [7]).

The time evolution of the total dissipation rate

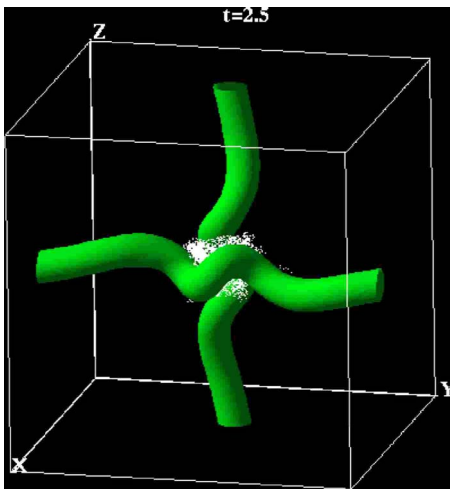


FIG. 6. (Color online) Isosurface plots of  $|\mathbf{B}|^2=27.3$  for IC-1. White dots:  $\det(\nabla\mathbf{A})=0.9995$  (8546 points).

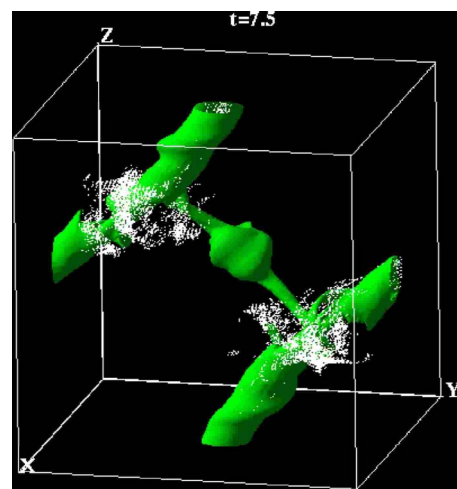


FIG. 8. (Color online) Isosurface plots of  $|\mathbf{B}|^2=7.87$  for IC-1. White dots:  $\det(\nabla\mathbf{A})=0.99$  (22 530 points).

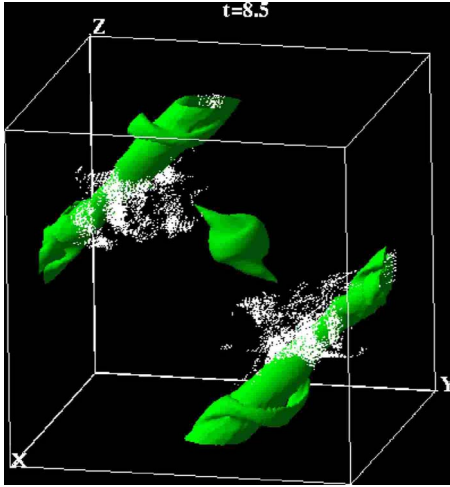


FIG. 9. (Color online) Isosurface plots of  $|\mathbf{B}|^2=6.05$  for IC-1. White dots:  $\det(\nabla\mathbf{A})=0.99$  (18 629 points).

$$\epsilon(t) = \nu \langle |\boldsymbol{\omega}|^2 + |\mathbf{J}|^2 \rangle$$

is plotted in Fig. 3. It shows a slow decay  $\epsilon(t) \approx 0.1$  during frequent resettings.

In order to characterize time scales more quantitatively, it is convenient to consider the time intervals between the adjacent resettings

$$\Delta t = t_j - t_{j-1}, \quad (j = 1, 2, \dots),$$

where  $t_j$  denote the time of  $j$ th resetting [6]. In Fig. 4 we show them for two different values of viscosity. Two features should be noted: first, the time scales are smaller for higher (magnetic) Reynolds number and second,  $\Delta t$  reaches a minimum around  $t=6$  and starts increasing again. It increases basically monotonically after the completion of reconnection around  $t=6$ .

It is of interest to study what physical events are associated with the resettings observed above. In Figs. 5–9, isosurfaces of  $|\mathbf{B}|^2$  are plotted together with locations of small  $\det(\nabla\mathbf{A})$  (white dots). All the isosurfaces plotted in this paper correspond to the case of  $\nu=2.0 \times 10^{-3}$ . (Note that out of resolved  $256^3$  grid points,  $128^3$  were used for visualization.)

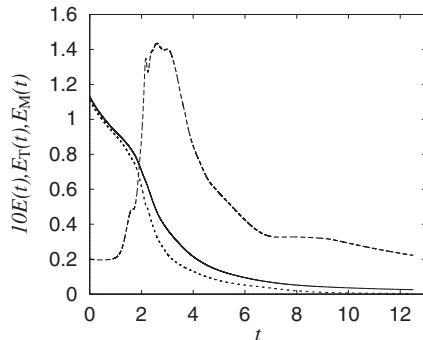


FIG. 10. Time evolution of the total energy  $E_T(t)$  (solid line), (ten times) the kinetic energy  $10E(t)$  (dashed), and the magnetic energy  $E_M(t)$  (dotted) for IC-2 with  $\nu=2.0 \times 10^{-3}$ .

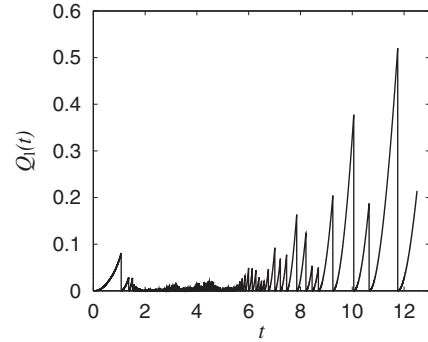


FIG. 11. Time evolution of spatial average of squared displacement for IC-2 with  $\nu=2.0 \times 10^{-3}$ .

From these plots we confirm that flux tubes indeed undergo magnetic reconnection on the time interval  $4 < t < 8$ , during which frequent resettings are taking place. It should be noted that at  $t=5.5$  and  $8.5$  the points with small  $\det(\nabla\mathbf{A})$  are found at the edges of a “bridge” joining the two flux tubes.

*IC-2: Antiparallel flux tubes with counterhelicity* [21]. This case was categorized as a “slingshot” in Ref. [13] (see its Fig. 9) and labeled “RL4” therein. In this case, we have oppositely signed helicity in the interaction zone. This configuration of countercochelicity enhances annihilation of helicity and releases magnetic energy efficiently.

We show in Fig. 10, the time development of three kinds of energies  $E_T(t)$ ,  $E_M(t)$ , and  $E_K(t)$  with the same convention as in Fig. 1. A very sharp peak in the kinetic energy  $E_K(t)$  centered around  $t=3$  is noticeable, followed by a rapid decay in magnetic energy  $E_M(t)$  and total energy  $E_T(t)$ . The kinetic energy  $E_K(t)$  takes relatively large values during the interval  $2 \leq t \leq 6$ , which is associated with a drop in the magnetic energy  $E_M(t)$ . This suggests that the magnetic energy is released through reconnection (to be confirmed by visualization below).

Indeed, the time development of the (squared) norm of displacement  $Q_s(t)$  in Fig. 11 shows frequent resettings just before  $t=2$  up to  $t=6$ . We note that this collapses on the interval of growth of kinetic energy, confirming that the resettings capture reconnection phenomena.

Figure 12 shows the time evolution of the dissipation rate of total energy  $\epsilon(t)$ , which is sharply peaked just past  $t=2$ .

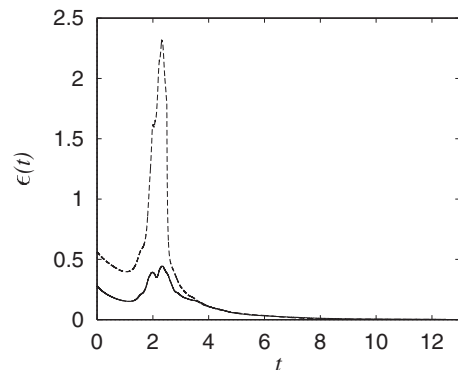


FIG. 12. Time evolution of dissipation of total energy for IC-2, with  $\nu=2.0 \times 10^{-3}$  (solid) and  $4.0 \times 10^{-3}$  (dashed).

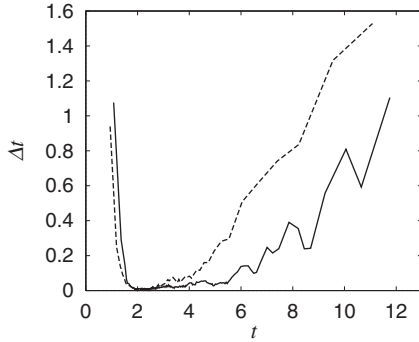


FIG. 13. Time evolution of resetting time scales for IC-2, plotted with the same line convention as in Fig. 12.

The magnetic energy released by reconnection leads to a sudden increase not only in kinetic energy (see Fig. 10), but also in the total dissipation.

The behavior of resetting time scale shown in Fig. 13. As in the previous case, it attains the minimum when the reconnection process starts and increases again after its completion.

In Figs. 14–17, we show the time evolution of the isosurfaces of the magnetic fields  $|\mathbf{B}|^2$ , together with regions with small  $\det(\nabla\mathbf{A})$ . We see clearly that prominent reconnection takes place between  $t=1.5$  and  $t=2.5$ . The regions with small determinants lie in the interaction zones where active reconnection is taking place.

*IC-3: Parallel flux tubes with cohesivity.* As the final case in three dimensions, we consider the case called a “merge” in Ref. [13] (see its Fig. 7) and labeled “RR0” therein. Note that here we have like-signed helicity in the interaction zone.

We see in Fig. 18 that the kinetic energy  $E_K(t)$  increases around  $t=2$ , with the decrease of the total  $E_T(t)$  energy and the magnetic energy  $E_M(t)$ . However, the increase is not so significant as compared with IC-2, because in this “merge” experiment annihilation of helicity is limited as a result of

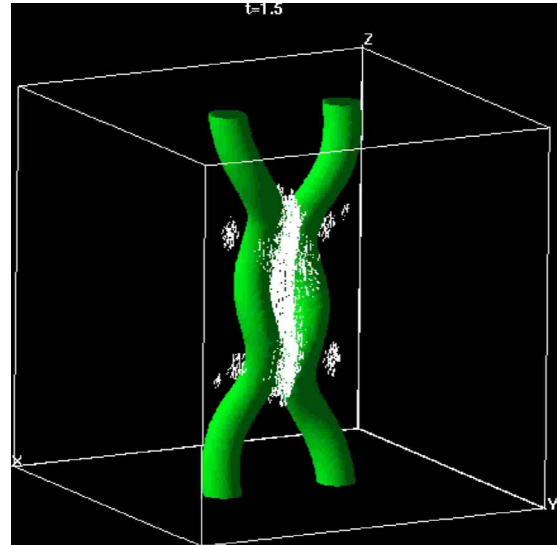


FIG. 15. (Color online) Isosurface plots of  $|\mathbf{B}|^2=32.3$  for IC-2. White dots show locations with small  $\det(\nabla\mathbf{A})=0.85$  (24 924 points).

the cohesivity configuration. It limits annihilation of helicity hence reducing the release of magnetic energy compared with IC-2 (see Fig. 10).

Even in this case we can still have frequent resettings in the time evolution of displacement  $Q_1(t)$  (Fig. 19), just before  $t=2$  to  $t=5$ . We note that the dissipation rate  $\epsilon(t)$  of the total energy is peaked when the kinetic energy increases rapidly (Fig. 20).

The resetting time scale attains minimum during  $2 \leq t \leq 4$  and then starts increasing later. The time scale is smaller for higher Reynolds number (Fig. 21).

In Figs. 22–25, we confirm that merging process is actively taking place during the frequent resettings, where two

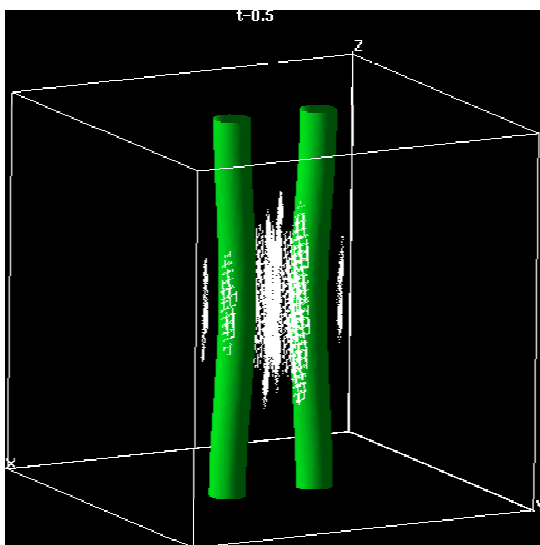


FIG. 14. (Color online) Isosurface plots of  $|\mathbf{B}|^2=39.8$  for IC-2. White dots show locations with small  $\det(\nabla\mathbf{A})=0.995$  (20 620 points).

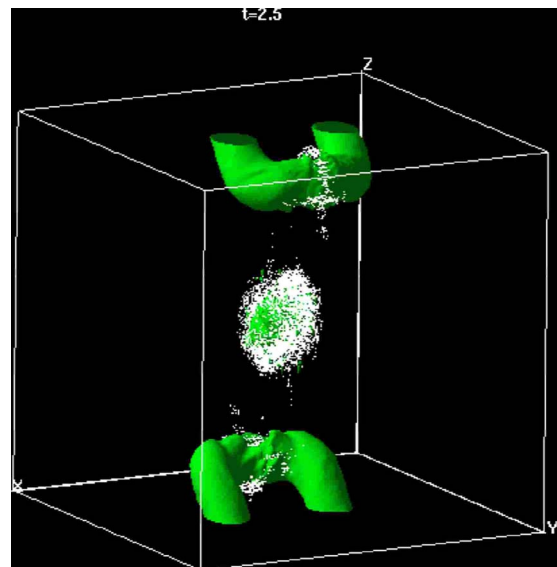


FIG. 16. (Color online) Isosurface plots of  $|\mathbf{B}|^2=14.6$  for IC-2. White dots show locations with small  $\det(\nabla\mathbf{A})=0.95$  (22 846 points).

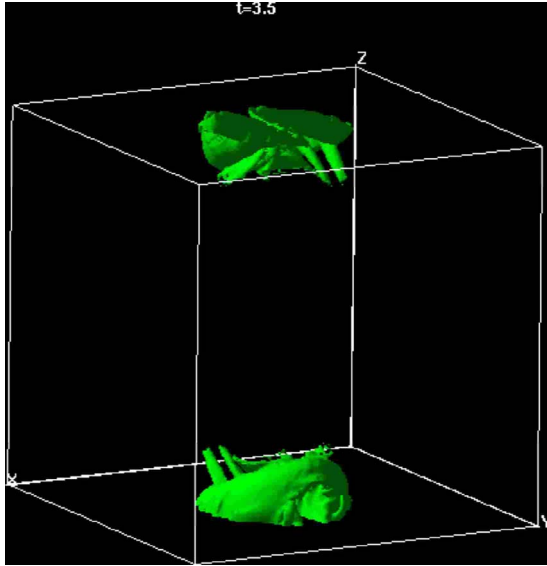


FIG. 17. (Color online) Isosurface plots of  $|B|^2=6.71$  for IC-2. No white dots are seen because they are plotted just after a resetting.

parallel right-handed flux tubes merge into a right-handed flux tube.

**C. Two-dimensional Orszag-Tang vortex**

Now we turn our attention to two-dimensional MHD equations. The governing equations in this case read

$$\frac{\partial \omega}{\partial t} + \mathbf{u} \cdot \nabla \omega = \mathbf{b} \cdot \nabla j + \nu \Delta \omega, \tag{23}$$

$$\frac{\partial a}{\partial t} + \mathbf{u} \cdot \nabla a = \nu \Delta a, \tag{24}$$

where

$$\mathbf{b} = (\partial_y a, -\partial_x a), \quad j = -\Delta a,$$

are the magnetic field and the current, respectively. The Eulerian-Lagrangian formulation for these equations are easily obtained by specializing the spatial dimension to two in what is given in the previous section.

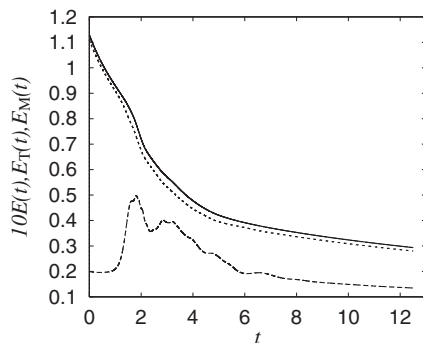


FIG. 18. Time evolution of the total energy  $E_T(t)$  (solid line), (ten times) the kinetic energy  $10E(t)$  (dashed), and the magnetic energy  $E_M(t)$  (dotted) for IC-3 with  $\nu=2.0 \times 10^{-3}$ .

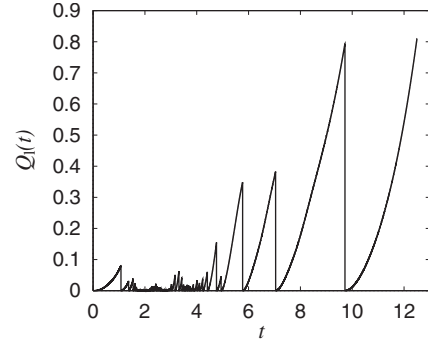


FIG. 19. Time evolution of spatial average of squared displacement for IC-3 with  $\nu=2.0 \times 10^{-3}$ .

As an initial condition, we choose so-called Orszag-Tang (OT) vortex defined by

$$\omega = -2(\cos x + \cos y)$$

and

$$a = 2 \cos x + \cos(2y).$$

We use  $512^2$  and  $1024^3$  grid points for 2/3-dealiased pseudospectral simulations. The values of kinematic viscosity used are  $\nu=\eta=5 \times 10^{-3}$  ( $512^2$  grid points) and  $2.5 \times 10^{-3}$  ( $1024^2$  grid points).

We take the maximum  $b_0=4$  in  $|\mathbf{b}|=4\sqrt{\sin^2 x + \sin^2(2y)}$  to estimate Alfvén velocity  $v_A=b_0/\sqrt{4\pi} \approx 1.28$ . We note that this initial condition was treated in Ref. [9], where the similar resettings were found at lower spatial resolutions of  $128^2$  grid points.

We show in Fig. 26 the time development of

$$E_I(t) = \frac{1}{2} \langle |I|^2 \rangle,$$

where the brackets denote a spatial average in  $[0, 2\pi]^2$ . It shows that frequent resettings take place. In Fig. 27, time development of the resetting time scales is shown. The general behavior is consistent with the results of Ref. [9], including a lack of clear decrease in the time scale.

We have examined the contours of the vector potential in order to show that magnetic reconnection actually corresponds to the resetting processes by investigating physical

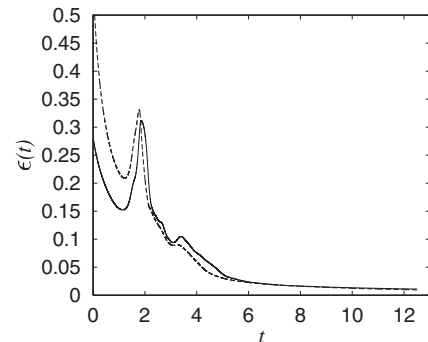


FIG. 20. Time evolution of dissipation of total energy for IC-3, with  $\nu=2.0 \times 10^{-3}$  (solid) and  $4.0 \times 10^{-3}$  (dashed).

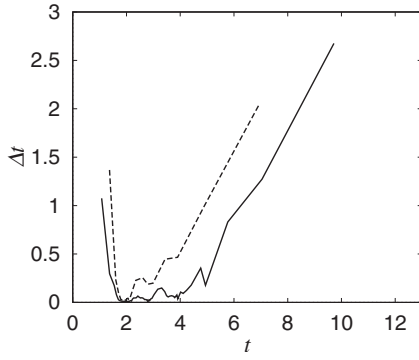


FIG. 21. Time evolution of resetting time scales for IC-3, plotted with the same line convention as in Fig. 20.

space structure. In Figs. 28 and 29, we plot time development of contours of magnetic potential  $a$ . We see that two magnetic vortices in the central region coalesce during a time interval of  $1.5 \leq t \leq 4.0$ . In that period of merging of  $a$ -islands, we have frequent resettings. Hence magnetic reconnection is well captured by resetting in two dimensional MHD as well.

A version of three-dimensional Orszag-Tang vortex was also studied in Ref. [9], where the resettings were found. Note also that resettings were found using similar three-dimensional initial conditions [19]. As stressed in Ref. [9], the resettings for these flows are correlated with growth magnetic energy and not with increase of the kinetic energy.

#### IV. SUMMARY AND DISCUSSION

Attempts have been made to characterize magnetic reconnection phenomena using the diffusive Lagrangian maps in the Eulerian-Lagrangian formalism. We generalize the Eulerian-Lagrangian formalism for Navier-Stokes equations

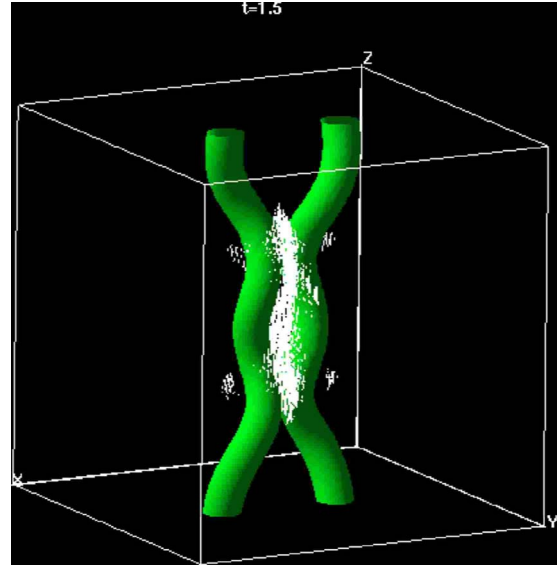


FIG. 23. (Color online) Isosurface plots of  $|\mathbf{B}|^2=32.3$  for IC-3. White dots show locations with small  $\det(\nabla\mathbf{A})=0.15$  (19 934 points).

to MHD case for the case of unit magnetic Prandtl number.

Our main objective here is to investigate reconnection, which releases magnetic energy into kinetic energy, on the basis of Eulerian-Lagrangian formalism. We compare orthogonally offset tubes and coelicity and counterhelicity configurations with twists along flux tubes.

In all the three different kinds of initial conditions in three dimension, we found the following features for the resetting time scale: it reaches a minimum and stays there for some time, during which significant reconnection proceeds and it starts to increase again approximately linearly in time. Therefore by plotting the time intervals of resettings, we can

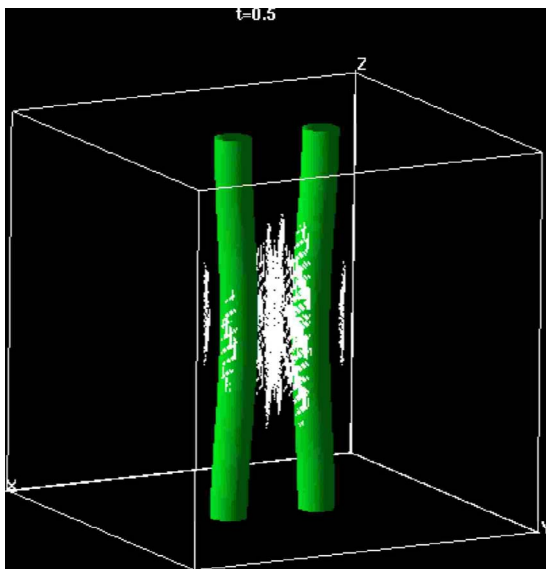


FIG. 22. (Color online) Isosurface plots of  $|\mathbf{B}|^2=39.8$  for IC-3. White dots show locations with small  $\det(\nabla\mathbf{A})=0.995$  (20 608 points).

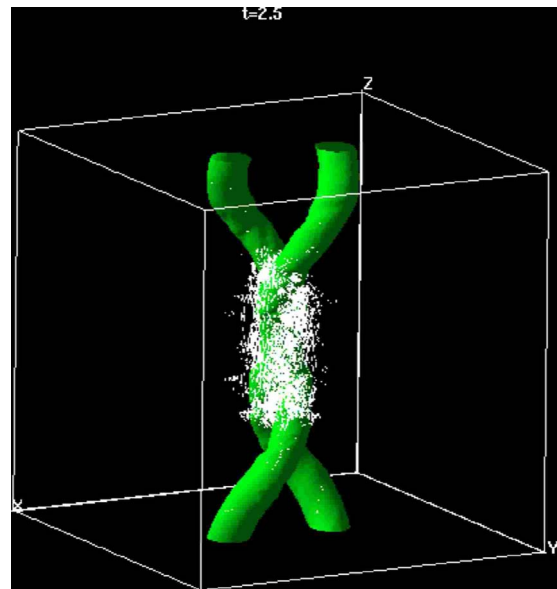


FIG. 24. (Color online) Isosurface plots of  $|\mathbf{B}|^2=23.7$  for IC-3. White dots show locations with small  $\det(\nabla\mathbf{A})=0.99$  (35 264 points).

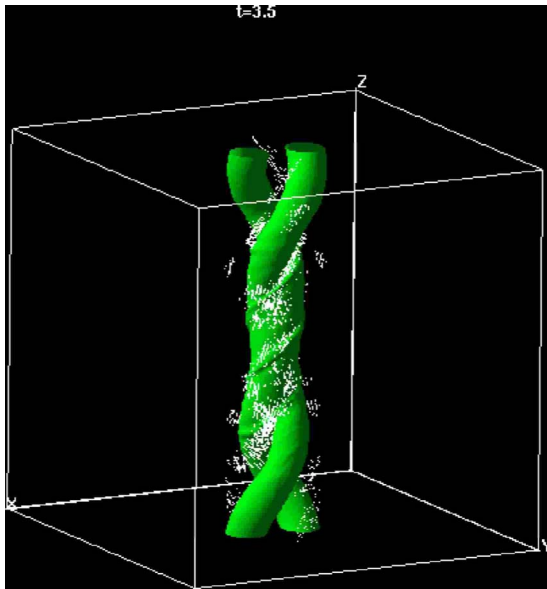


FIG. 25. (Color online) Isosurface plots of  $|B|^2=19.4$  for IC-3. White dots show locations with small  $\det(\nabla A)=0.999$  (20 859 points).

tell when the substantial resetting takes place reasonably well.

In three dimensions, we consider cases where flux tubes are highly localized in space. Two facts should be noted regarding the advantages of the Eulerian-Lagrangian approach. (i) The spatial regions with small values of the determinant  $\det(\nabla A)$  coincide with locations of active magnetic reconnection (as confirmed by visualization of flux tubes). (ii) Short time scales are found by resettings of  $\det(\nabla A)$ , and they come from those localized region in (i). Thus, as far as the present numerical experiments are concerned, it makes sense to associate the time scale with the magnetic reconnection. In other words, the Eulerian-Lagrangian analyses allow us to extract the time scale of reconnection inductively.

Finally, a few comments on the models of magnetic reconnection may be in order. Regarding two-dimensional models, such as Sweet-Parker's and Petschek's, there had been discussions on whether steady self-consistent solutions can yield reconnection that are localized in both directions.

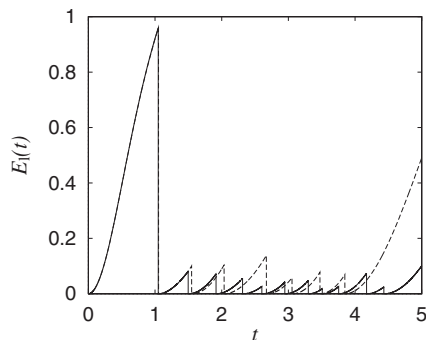


FIG. 26. Time evolution of displacement norm: Solid line ( $\eta = 2.5 \times 10^{-3}$ ) and dashed ( $5 \times 10^{-3}$ ).

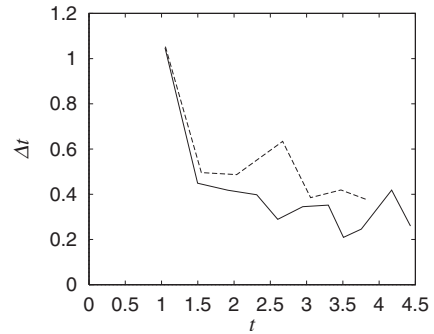


FIG. 27. Comparison of resetting time scales for OT vortex, plotted with the same line convention as in Fig. 26.

The Sweet-Parker model is a solution that is only localized in one spatial direction with throttled reconnection. The Petschek model for the same configuration used to be regarded as providing an unthrottled solution. It was later found that the result is not a solution of the resistive MHD equations [3]. Studies over the past decade have focused on non-MHD effects that do yield Petschek-like localization, but these solutions are not reproduced by resistive MHD, e.g., Ref. [20]. In this paper, the problem setting produces localized structures as initial conditions, hence faster reconnection. Whether the method will also be useful in obtaining spontaneous localization, which is different from the cases described here, is left for future study.

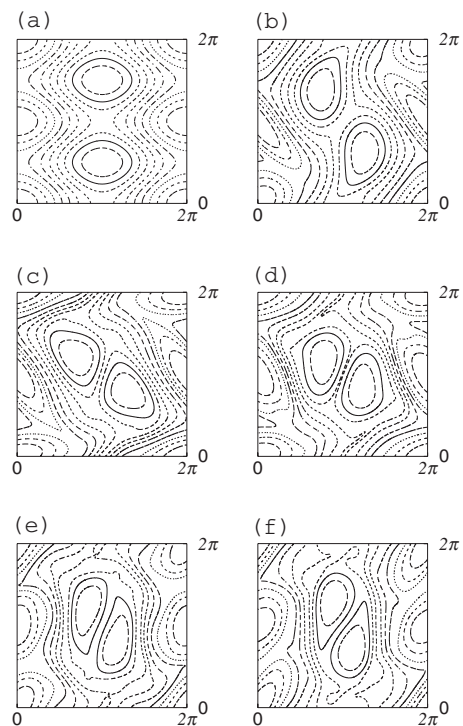


FIG. 28. Time evolution of contours of magnetic potential plotted with ten equally separated levels, for (a)  $t=0$ , (b)  $t=0.5$ , (c)  $t=1.0$ , (d)  $t=1.5$ , (e)  $t=2.0$ , and (f)  $t=2.5$ .

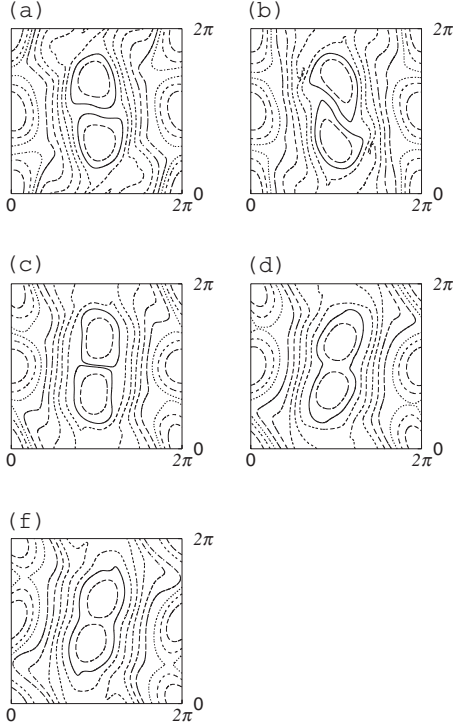


FIG. 29. Time evolution of contours of magnetic potential plotted with ten equally separated levels, for (a)  $t=3.0$ , (b)  $t=3.5$ , (c)  $t=4.0$ , (d)  $t=4.5$ , and (e)  $t=5.0$ .

#### ACKNOWLEDGMENTS

One of the authors (K.O.) has been supported by the Royal Society and from an EPSRC Grant No. EP/F009267/1. Part of this work was done while K.O. was affiliated with Research Institute for Mathematical Sciences, Kyoto University. It has been partially supported by Grant-in-Aid for scientific research from the Ministry of Education, Culture, Sports, Science and Technology of Japan, under Grant No. 16540103, 2004–2005. The authors have been benefited from a referee's explanation on the models of magnetic reconnection.

#### APPENDIX: IDEAL MHD IN THREE DIMENSIONS

We first review Weber transforms in ideal MHD [17,18]. The governing equations for velocity  $\mathbf{u}$ , magnetic field  $\mathbf{B}(\mathbf{B}=\nabla\times\mathcal{A})$  read

$$\frac{D\mathbf{u}}{Dt} = -\nabla p + (\nabla\times\mathbf{B})\times\mathbf{B}, \quad (\text{A1})$$

$$\frac{\partial\mathbf{B}}{\partial t} = \nabla\times(\mathbf{u}\times\mathbf{B}), \quad (\text{A2})$$

where  $\nabla\cdot\mathbf{u}=\nabla\cdot\mathbf{B}=0$ . Note that  $\mathcal{A}$  is the magnetic potential, not diffusive labels.

The second can be written as

$$\frac{\partial\mathcal{A}}{\partial t} = \mathbf{u}\times(\nabla\times\mathcal{A}) - \nabla\phi \quad (\text{A3})$$

or

$$\frac{D\mathcal{A}}{Dt} = -\mathcal{A}(\nabla\mathbf{u})^T - \nabla\chi, \quad (\text{A4})$$

where  $p$ ,  $\chi=\varphi-\mathbf{u}\cdot\mathcal{A}$  are scalars and  $T$  denotes matrix transpose.

There are two kinds of helicity-like conservation laws: magnetic helicity and cross-helicity

$$\int \mathcal{A}\cdot\mathbf{B}dx, \int \mathbf{u}\cdot\mathbf{B}dx.$$

To each conservation law there corresponds Weber-like transform.

Under the choice of gauge  $\nabla\cdot\mathcal{A}=0$  The Weber transform for the former is derived from

$$\frac{D}{Dt}\left(\mathcal{A}_i\frac{\partial x_i}{\partial a_k}\right) = -\frac{\partial\chi}{\partial a_k} \quad (\text{A5})$$

as

$$\mathcal{A}_i = \mathcal{A}_i(0)\frac{\partial a_k}{\partial x_i} - \frac{\partial\Phi}{\partial x_i}, \quad \Phi = \int_0^t \chi(\mathbf{a}, t')dt', \quad (\text{A6})$$

or

$$\mathcal{A} = P[\mathcal{A}_0(\nabla\mathbf{a})^T], \quad (\text{A7})$$

where  $\mathbf{a}$  is Lagrangian label and  $P$  solenoidal projection.

For the second cross-helicity, we describe a derivation of the corresponding Weber transform [18] ( $\mathbf{J}=\nabla\times\mathbf{B}$ )

$$\frac{D\mathbf{u}}{Dt}\cdot\frac{\partial\mathbf{x}}{\partial a_i} = -\frac{\partial p}{\partial a_i} - (\mathbf{B}\times\mathbf{J})\cdot\frac{\partial\mathbf{x}}{\partial a_i}. \quad (\text{A8})$$

The left hand side is as usual,

$$\frac{D\mathbf{u}}{Dt}\cdot\frac{\partial\mathbf{x}}{\partial a_i} = \frac{D}{Dt}\left(\mathbf{u}\cdot\frac{\partial\mathbf{x}}{\partial a_i}\right) - \frac{\partial}{\partial a_i}\frac{|\mathbf{u}|^2}{2}. \quad (\text{A9})$$

For the right-hand side, we introduce an auxiliary variable  $\mathbf{m}$  by

$$\frac{D\mathbf{m}}{Dt} = \mathbf{m}\cdot\nabla\mathbf{u} + \mathbf{J}, \quad (\text{A10})$$

$$\nabla\cdot\mathbf{m} = 0, \quad (\text{A11})$$

which satisfies

$$\frac{D(\mathbf{m}\cdot\delta\mathcal{S})}{Dt} = \mathbf{J}\cdot\delta\mathcal{S} \quad (\text{A12})$$

for any surface element  $\delta\mathcal{S}$ . Then

$$\begin{aligned}
(\mathbf{B} \times \mathbf{J}) \cdot \frac{\partial \mathbf{x}}{\partial a_i} &= \left( \frac{\partial \mathbf{x}}{\partial a_i} \times \mathbf{B} \right) \cdot \mathbf{J} = \frac{D}{Dt} (\mathbf{m} \cdot \delta \mathbf{S}) \\
&= \frac{D}{Dt} \left[ \mathbf{m} \cdot \left( \frac{\partial \mathbf{x}}{\partial a_i} \times \mathbf{B} \right) \right] = \frac{D}{Dt} \left( (\mathbf{B} \times \mathbf{m}) \cdot \frac{\partial \mathbf{x}}{\partial a_i} \right),
\end{aligned}$$

so

$$\frac{D}{Dt} \left( \mathbf{u} \cdot \frac{\partial \mathbf{x}}{\partial a_i} \right) = \frac{\partial}{\partial a_i} \left( \frac{|\mathbf{u}|^2}{2} - p \right) - \frac{D}{Dt} \left( (\mathbf{B} \times \mathbf{m}) \cdot \frac{\partial \mathbf{x}}{\partial a_i} \right).$$

Introducing a generalized velocity

$$\tilde{\mathbf{u}} \equiv \mathbf{u} + \mathbf{B} \times \mathbf{m}, \quad (\text{A13})$$

$\tilde{\mathbf{u}}$  satisfies

$$\frac{D}{Dt} \left( \tilde{\mathbf{u}} \cdot \frac{\partial \mathbf{x}}{\partial a_i} \right) = \frac{\partial}{\partial a_i} \left( \frac{|\mathbf{u}|^2}{2} - p \right). \quad (\text{A14})$$

The corresponding Weber transform is

$$\mathbf{u} = \mathbf{P}[\tilde{\mathbf{u}}_0(\mathbf{a})(\nabla \mathbf{a})^T + \mathbf{m} \times \mathbf{B}]. \quad (\text{A15})$$

Note that Weber transform for MHD is not kinematic, because  $\mathbf{m}$  depends on history of evolution, as is seen by the following formula:

$$m_i = \left( m_j(0) + \int_0^t J_k(\mathbf{a}, t') \frac{\partial a_j}{\partial x_k} dt' \right) \frac{\partial x_i}{\partial a_j}. \quad (\text{A16})$$

We also note that the governing equations for  $\tilde{\mathbf{u}}$  and generalized vorticity  $\tilde{\boldsymbol{\omega}} = \nabla \times \tilde{\mathbf{u}}$  are

$$\frac{D\tilde{\mathbf{u}}}{Dt} = -\nabla p - (\mathbf{B} \times \mathbf{m}) \cdot (\nabla \mathbf{u})^T \quad (\text{A17})$$

and

$$\frac{D\tilde{\boldsymbol{\omega}}}{Dt} = (\tilde{\boldsymbol{\omega}} \cdot \nabla) \mathbf{u}, \quad (\text{A18})$$

respectively.

- 
- [1] E. Priest and T. Forbes, *Magnetic Reconnection* (Cambridge University Press, Cambridge, 2000).
- [2] E. N. Parker, *Spontaneous Current Sheets in Magnetic Fields: With Applications to Stellar X Rays* (Oxford University Press, Oxford, 1994).
- [3] D. Biskamp, *Nonlinear Magnetohydrodynamics* (Cambridge University Press, Cambridge, 1993).
- [4] P. Constantin, *Commun. Math. Phys.* **216**, 663 (2001).
- [5] P. Constantin, in *Handbook of Mathematical Fluid Dynamics*, edited by S. Friedlander and D. Serre (Elsevier, Amsterdam, 2003), Vol. 2, pp. 117–141.
- [6] K. Ohkitani and P. Constantin, *Phys. Fluids* **15**, 3251 (2003).
- [7] K. Ohkitani and P. Constantin, *Phys. Fluids* **20**, 075102 (2008).
- [8] C. Cartes, M. Bustamante, and M. E. Brachet, *Phys. Fluids* **19**, 077101 (2007).
- [9] C. Cartes, M. D. Bustamante, A. Pouquet, and M. E. Brachet, *Fluid Dyn. Res.* (to be published).
- [10] T. Gold and F. Hoyle, *Mon. Not. R. Astron. Soc.* **120**, 89 (1960).
- [11] R. B. Dahlburg and S. K. Antiochos, *J. Geophys. Res.* **100**, 16991 (1995).
- [12] M. G. Linton and E. R. Priest, *Astrophys. J.* **595**, 1259 (2003).
- [13] M. G. Linton, R. B. Dahlburg, and S. K. Antiochos, *Astrophys. J.* **553**, 905 (2001).
- [14] R. B. Dahlburg and D. Norton, *Lect. Notes Phys.* **462**, 331 (1995).
- [15] A. Brandenburg and R. M. Kerr, *Lect. Notes Phys.* **571**, 358 (2001).
- [16] O. N. Boratav, R. B. Pelz, and N. J. Zabusky, *Phys. Fluids A* **4**, 581 (1992).
- [17] V. E. Zakharov and E. A. Kuznetsov, *Dokl. Akad. Nauk SSSR* **194**, 1288 (1970) [*Sov. Phys. Dokl.* **15**, 913 (1971)].
- [18] V. A. Vladimirov and K. H. Moffatt, *J. Fluid Mech.* **283**, 125 (1995).
- [19] K. Ohkitani and P. Constantin, *RIMS Kokyuroku* **1434**, 116 (2005).
- [20] J. Birn *et al.*, *J. Geophys. Res.* **106**, 3715 (2001).
- [21] The case of antiparallel flux tubes with cohelicity (RR4) and that of parallel flux tubes with counterhelicity (RL0) result in a “bounce” without significant reconnection.